NANO LETTERS

pubs.acs.org/NanoLett

Letter

What Determines the Critical Electric Field of AFE-to-FE in $Pb(Zr,Sn,Ti)O_3$-Based Perovskites?

Botao Gao, Wenjie Zhou, Hui Liu,* He Qi, Shiqing Deng, Shi Liu,* and Jun Chen*

Cite This: *Nano Lett.* 2023, 23, 948−953

Read Online

ABSTRACT: Electric-field-induced antiferroelectric-ferroelectric (AFE-FE) phase transition is a prominent feature of antiferroelectric (AFE) materials. The critical electric field of this phase transition is crucial for the device performance of AEFs in many applications, but the determining factor of the critical electric field is still unclear. Here, we have established the correlation between the underlying structure and the critical electric field by using *in situ* synchrotron X-ray diffraction and high-resolution neutron diffraction in $Pb(Zr,Sn,Ti)O_3$-based antiferroelectrics. It is found that the critical electric field is determined by the angle between the average polarization vector in the incommensurate AFE state and the $[111]_P$ polarization direction in the rhombohedral FE state. A large polarization rotation angle gives rise to a large critical electric field. Further, density functional theory (DFT) calculations corroborate that the lower energy is required for driving a smaller angle polarization rotation. Our discovery will offer guidance to optimize the performance of AFE materials.

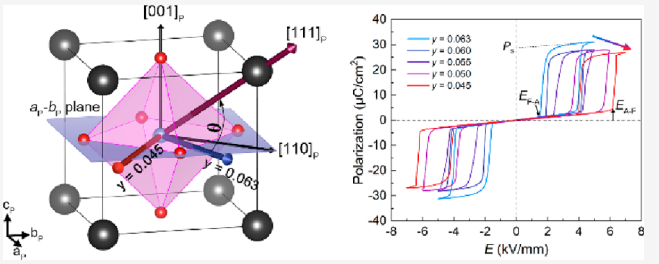

KEYWORDS: *Incommensurate structure, $PbZrO_3$-based antiferroelectric, dipole configuration, perovskite, dipole rotation*

Electric field driven polarization switching, typically characterized by the macroscopic hysteresis loop, is the foundation of the various applications in dielectric materials. In ferroelectrics (FEs), the critical electric field for polarization reversal, termed the coercive field (E_C), has significant influence on the functional properties of FE materials. Analogously, AFEs present a critical electric field, which represents the phase switching point between an AFE-phase and a FE-phase induced by the electric field. At the critical electric field of AFEs, a large macroscopic polarization develops and significant volume change typically occurs. The manifestation of these parameters allows AFE materials to be exploited for use in transducers, energy storage devices, and so on.[1] Particularly, the critical electric field is an important parameter for AFE devices. For example, a small critical electric field is required for the application as a driver[2] while a large one is beneficial to improve the energy storage density of capacitors.[3] Therefore, revealing the underlying mechanism of critical electric field of AFEs is crucial to design high performance materials.

Previous studies have found that AFEs with different chemical compositions exhibit different critical electric fields, and it is attributed to the strength of the FE order.[4] In contrast to the extensive studies on the E_C of FEs,[5,6] few studies involved the underlying structure mechanism in the critical electric fields of AFEs. Milesi-Brault et al.[7] investigated the rotation behavior of the typical AFE $PbZrO_3$ thin film, and they found that the critical electric field is highly dependent on the direction of applying electric field. Fu et al.[8] and Ma et al.[9] investigated the chemical modified lead-based AFEs using electron microscopy, and they found that the critical electric field is related to the characteristic of the incommensurate structure. Recently, our group revealed some new incommensurate modulated dipole configurations in AFEs.[10,11] Inspired by these results, we suppose that the critical electric field may be related to the polarization rotation based on the modulation dipole configurations.

In this work, by investigating a series of lead-based AFEs with different critical electric field ($Pb_{0.99}Nb_{0.02}[(Zr_{0.53}Sn_{0.47})_{1-y}Ti_y]_{0.98}O_3$, $0.045 \leq y \leq 0.063$) using advanced diffraction techniques, the relationship between the modulated dipole configuration and the critical electric field was revealed. It is found that there is a polarization jump rotation from the modulated dipole configuration (in the a_P-b_P plane) to the $[111]_P$ direction, and this rotation leads to the critical electric field. Interestingly, the critical electric field strongly correlates with the rotation angle θ between the average polarization vector and the $[111]_P$ direction. A large θ leads to a large critical electric field. The DFT calculations confirm that a small rotation angle

Received: November 7, 2022
Revised: December 30, 2022
Published: January 30, 2023

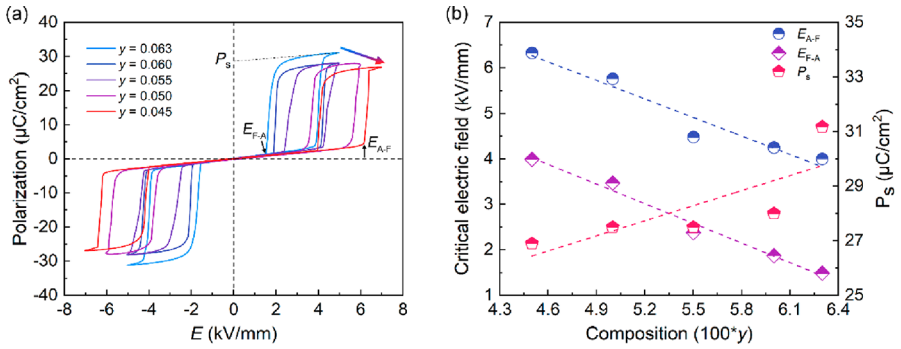

Figure 1. (a) $P-E$ loops for the $Pb_{0.99}Nb_{0.02}[(Zr_{0.53}Sn_{0.47})_{1-y}Ti_y]O_3$ ceramics measured at room temperature. (b) The critical electric fields and the P_s as a function of composition y in $Pb_{0.99}Nb_{0.02}[(Zr_{0.53}Sn_{0.47})_{1-y}Ti_y]O_3$ ceramics.

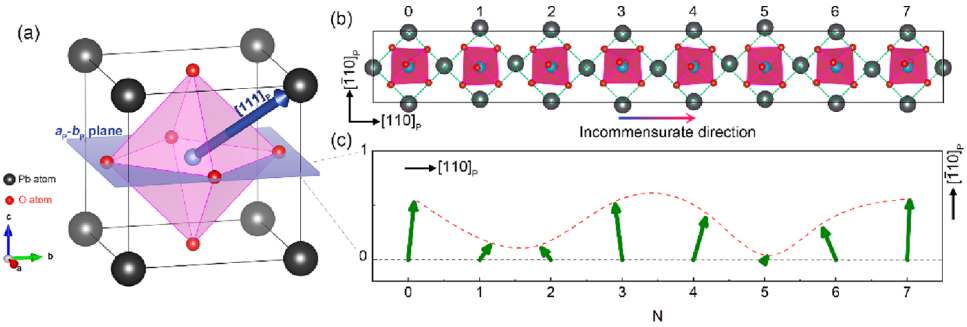

Figure 2. (a) Schematic diagram of a perovskite cell. (b) Supercell schematic of $Pb_{0.99}Nb_{0.02}[(Zr_{0.53}Sn_{0.47})_{0.937}Ti_{0.063}]O_3$. (c) 2D-dipole configuration of $Pb_{0.99}Nb_{0.02}[(Zr_{0.53}Sn_{0.47})_{0.937}Ti_{0.063}]O_3$.

corresponds to a small energy barrier. These results will deepen the understanding of AFE theory and enlighten the future design of AFE materials.

Several $PbZrO_3$-based AFE ceramics in stoichiometry of $Pb_{0.99}Nb_{0.02}[(Zr_{0.53}Sn_{0.47})_{1-y}Ti_y]_{0.98}O_3$ (y = 0.045, 0.05, 0.055, 0.060, and 0.063) have been fabricated by the solid-state method. The details of the synthesis are shown in Supporting Information. The polarization vs electric field hysteresis loops ($P-E$ loops) were collected at room temperature. As shown in Figure 1a, all the samples exhibit well-defined double hysteresis loops and zero remanent polarization (P_r), indicating a typical characteristic of AFEs. In AFEs, the critical electric field (phase switching field) from the AFE state to the FE state is defined as E_{A-F} and the backward switching field is defined as E_{F-A} (Figure 1a). As shown in Figure 1b, upon increasing the Ti content from 0.045 to 0.063, E_{A-F} decreased from ~6.3 kV/mm to ~4.0 kV/mm, E_{F-A} decreased from ~4.0 kV/mm to ~1.5 kV/mm, while saturated polarization (P_s) increased from ~26.9 $\mu C/cm^2$ to ~31.2 $\mu C/cm^2$. This phenomenon also has been observed in other literature.[12] In order to acquire the internal structure evidence, an in-depth structural analysis is required.

The Nb-doped Pb(Zr,Sn,Ti)O_3 AFE systems were reported to have complex incommensurate structures,[13,14] which are related to the atomic displacement and the tilting of the oxygen octahedra.[15] The difficulties in the analysis of the incommensurate structure lie in the determination of the superspace group and the oxygen atom position. The determination of the superspace group can be referred to our previous work,[10] and the high-resolution neutron powder diffraction (HR-NPD) was adopted, combined with Rietveld refinement, to unveil the oxygen atom position. In this way, the precise crystallographic parameters can be obtained.

After careful refinement for the HR-NPD data of different AFEs, all the patterns (Figure S1) show a good agreement with the experiment. The precise crystallographic parameters are shown in Tables S1−S5. It can be seen that with increasing Ti content, the change of the cell parameters is very small (Figure S2a), suggesting that there is no relationship between the critical electric field and the cell parameters. By comparison, the magnitude of modulated vector **q** gradually decreases with the increase of Ti content, and this trend is the same as the critical electric field (Figure 1b). This phenomenon is also observed by using selected area electron diffraction.[8] For incommensurate modulated structure in this case, the decrease of **q** represents the increase of modulated period along the $[110]_P$ direction. It is well-known that the prototype lead-based AFE $PbZrO_3$ is equivalent to a perovskite with a commensurate structure of $1\{110\}_P$, i.e., a four layer periodic dipole configuration (two dipoles remain in the same direction in a period),[16−19] and compared to the chemical-doped modulated AFEs, in which more dipoles remain same direction in a period, the dipoles in $PbZrO_3$ are more difficult to be switched under an electric field. Therefore, pure $PbZrO_3$ always has an extremely high critical electric field.

In order to investigate the relationship between the dipole configuration and the critical electric field, all dipole configurations were quantitatively analyzed. Here, we took one of the five chemical compositions (y = 0.063) as an example to show their dipole configuration in the a_P-b_P plane (Figure 2a). The detailed analysis process and theory can be found elsewhere.[10] The approximate supercell of $Pb_{0.99}Nb_{0.02}[(Zr_{0.53}Sn_{0.47})_{0.937}Ti_{0.063}]O_3$ is shown in Figure 2b. The shift of Pb atoms and the tilting of oxygen octahedra present a modulated feature. It indicates that the incommensurate structure is attributed to the coupling between the

https://doi.org/10.1021/acs.nanolett.2c04361
Nano Lett. 2023, 23, 948−953

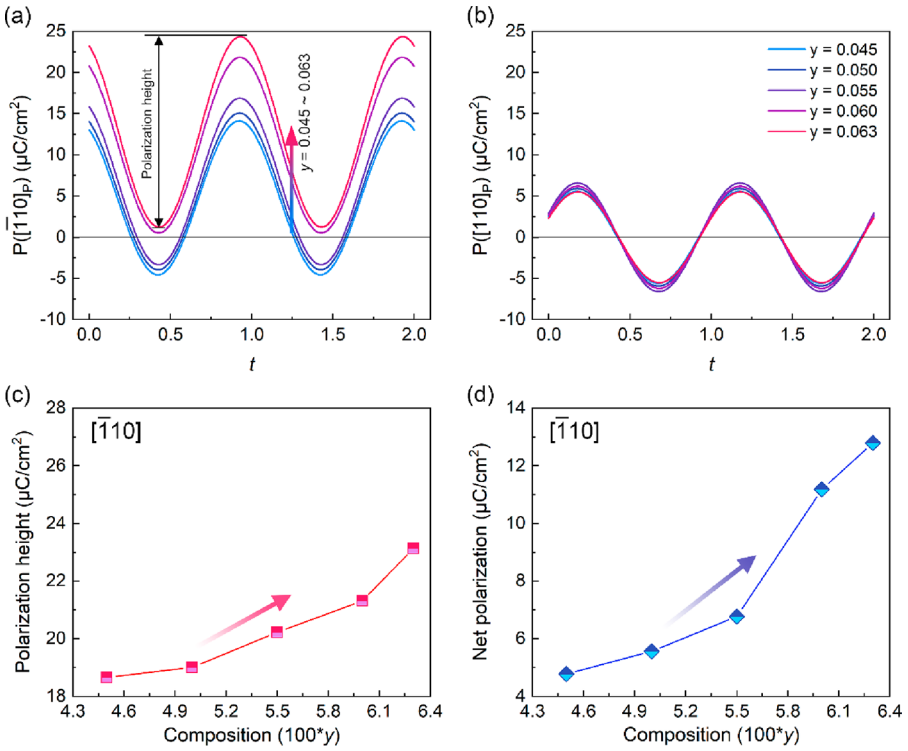

Figure 3. (a) Polarization component along $[\bar{1}10]_P$. (b) Polarization component along $[110]_P$ direction. (c) Polarization magnitude (maximum local polarization minus minimum local polarization in the $[\bar{1}10]_P$ direction). (d) Net polarization (the integral area of each curve in part a) in $[\bar{1}10]_P$ direction. The physical meaning of t can be found in Supporting Information.

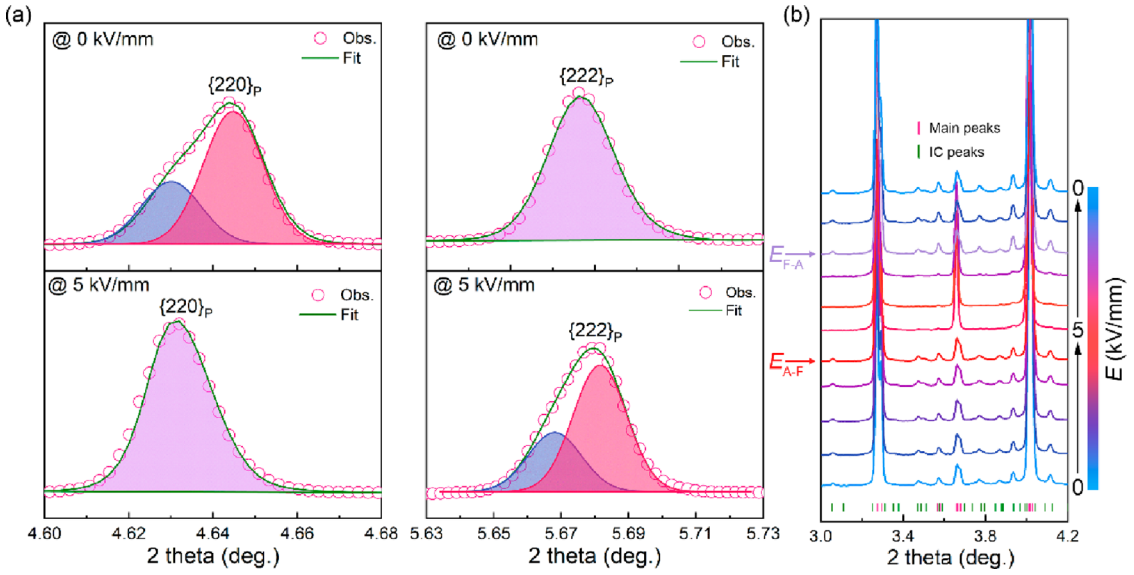

Figure 4. (a) Fitted 45° sector diffraction peaks of $\{220\}_P$ and $\{222\}_P$ at 0 kV/mm and 5 kV/mm. (b) Evolution of incommensurate (IC) peaks as a function of the bipolar electric field at 45° sector.

atomic displacement and the oxygen octahedra tilting. The 2D-dipole configuration is shown in Figure 2c, and each arrow represents a dipole in a perovskite in Figure 2b. Evidently, the magnitude and angle of dipoles gradually change along the incommensurate direction of $[110]_P$. Hence, dipoles are not strictly parallel to the $[\bar{1}10]_P$ direction, and the polarization cannot be fully compensated in the $[\bar{1}10]_P$ direction. Compared to pure $PbZrO_3$, the AFE with this kind of dipole configuration has a smaller critical electric field. This requires us to reunderstand the structure−property correlation of AFE materials.

In order to compare the polarization of different AFEs, the polarization components along the $[\bar{1}10]_P$ direction (perpendicular to the incommensurate direction) and the $[110]_P$ direction (parallel to the incommensurate direction) are shown in Figure 3a and Figure 3b, respectively. Apparently, the polarization components in two directions all present a sinusoidal-wave feature. In particular, the $[\bar{1}10]_P$ direction presents a dominating polarization compared to the $[110]_P$

https://doi.org/10.1021/acs.nanolett.2c04361
Nano Lett. 2023, 23, 948−953

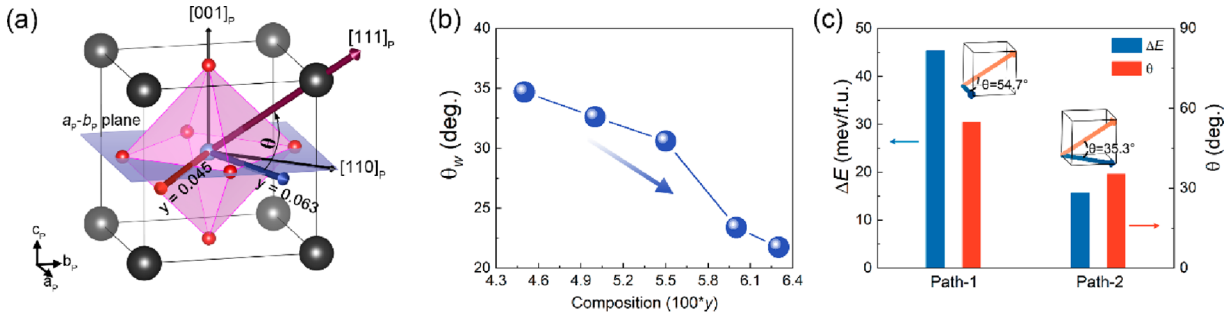

Figure 5. (a) Schematic of rotation angle θ. (b) Rotation angle θ_w as a function of the composition y. It is worth noting that the θ_w is not an angle in the normal sense; that is why it will less than 35.2°. (c) DFT calculated energies with respect to different polarization rotation paths: Path-1, $[100]_P \rightarrow [111]_P$; Path-2, $[110]_P \rightarrow [111]_P$.

direction. As seen in Figure 3a, with the increase of Ti content, the polarization−t curves move up, which indicates that the local polarization is enhanced. For example, the maximum local polarization increases from ∼14 μC/cm^2 to ∼24 μC/cm^2 when the Ti content increases from 0.045 to 0.063. However, the polarization in the $[110]_P$ direction is relatively stable, and the maximum local polarization is between 6 and 7 μC/cm^2. It indicates that the change of Ti content has little effect on the polarization in the $[110]_P$ direction. The polarization height (maximum local polarization minus minimum local polarization) and the net polarization along the $[\bar{1}10]_P$ direction, extracted from Figure 3a, are shown in Figure 3c,d. Both the polarization height and net polarization are increasing with the increase of Ti content. This implies the enhancement of ferroelectricity with the increase of Ti content. As expected, the saturation polarization also increases with the Ti content increasing (Figure 1a). It suggests a strong dependence between the microscopic local polarization and the macroscopic saturation polarization. The ferroelectricity at the zero electric field represents the potential ability to be induced into a ferroelectric state under the high electric field. In other words, the ferroelectricity at the ground state will be released at the high electric field; hence the AFE with the higher net polarization or the polarization height tends to have higher saturation polarization.

To probe the crystal structure evolution under the electric field, synchrotron radiation *in situ* experiment was applied on the sample of Ti content of 0.063. The details of the data collection can be found in our previous work.[20] Previous experiments showed that the data of the 45° sector have a negligible texture effect, so it is suitable to study the phase transition process. The pseudo-Voigt peaks were used to fit the $\{220\}_P$ or the $\{222\}_P$ peaks. As shown in Figure 4a, at 0 kV/mm, the $\{220\}_P$ peak shows an obvious splitting feature, while the $\{222\}_P$ peak does not. This is the typical characteristic of the orthorhombic phase (O phase), which is consistent with the HR-NPD refinement results. Oppositely, the $\{222\}_P$ peak at 5 kV/mm shows a splitting feature, while the $\{220\}_P$ peak does not, which shows a typical characteristic of the rhombohedral phase (R phase). This suggests that the structure evolution induced by the electric field is from O phase to R phase. The incommensurate peaks (IC peaks) also show an interesting evolution (as seen in Figure 4b). The IC peaks appear at the low electric field and disappear at the high electric field. When the electric field is gradually removed, the IC peaks appear again. Particularly, this evolution is very drastic, and the IC peaks do not change before the electric field reaches E_{A-F}. Beyond the E_{A-F}, IC peaks disappear suddenly. The opposite process also occurs around the E_{F-A}. This drastic change is consistent with the jump change of the polarization near the critical electric field of the hysteresis loops (Figure 1a).

To further verify the precise structure under different electric fields, the Rietveld refinement was carried out on the data of two electric fields (0 kV/mm and 5 kV/mm). The result of the refinement shows a great agreement with the observed data (Figure S3, Table S6). Therefore, the electric-field-induced phase transition is identified and this phase transition can be attributed to the polarization rotation from incommensurate O phase to R phase in AFEs. It is worth noting that the polarization rotation is also reported in FE systems.[21−23] To describe the difference in the polarization rotation of the different AFEs, a rotation angle was proposed in this case.

The schematic of the rotation angle, θ, is shown in Figure 5a. It represents the angle between the initial dipole and the $[111]_P$ direction. As mentioned early, the dipole configuration at ground state is modulated, so the direction of dipoles are not strictly along the $[\bar{1}10]_P$ direction (Figure 2b). Therefore, the average θ in one period was used to describe the rotation angle of an AFE. Considering that the magnitude of the dipoles also affects the critical electric field, a weight factor w was defined to quantify the influence of the dipole magnitude. Consequently, the θ_w can be calculated by the following formula:

$$\theta_w = \frac{\sum_{i=1}^{N} \theta_i w_i}{N} \tag{1}$$

where the θ_i represents the angle between the ith dipole vector and $[111]_P$ direction, the N represents the number of the perovskite cells in one period, in this case, N = 100, and the w_i represents the weight factor of the ith dipole vector. It can be estimated by the following formula:

$$w_i = \frac{m_i}{m_{max}} \tag{2}$$

where the m_i represents the magnitude of the ith dipole vector, and the m_{max} represents the maximum magnitude of the dipoles.

Considering the synergistic effect and lowest-energy principle, it is necessary to state the basis of the calculation here. First, for an orthorhombic AFE, under the electric field, the polarization always tends to rotate to the same terminal $\langle 111\rangle_P$ direction in a long-range. Otherwise, there is a large stress gradient between two adjacent perovskites, which is unstable (Figure S4). Second, there are four $\langle 111\rangle_P$ directions ($[\bar{1}11]_P$, $[1\bar{1}1]_P$, $[\bar{1}\bar{1}1]_P$, and $[111]_P$) that may become the

https://doi.org/10.1021/acs.nanolett.2c04361
Nano Lett. 2023, 23, 948−953

terminal direction; i.e., there are four paths, but the rotation angle must be the smallest one to ensure the energy cost is lowest. On this base, the rotation angle θ_w as a function of composition y is shown in Figure 5b. Interestingly, with increasing composition y, the θ_w decreases gradually. This trend is consistent with the critical electric field (Figure 1b). This result indicates that the critical electric field is highly dependent on the rotation path of dipoles, which means a larger value of θ_w indicates a stronger critical field. This conclusion can also be supported by the following facts. The E_c of rhombohedral FE (R-phase FE), in which the dipole need rotate 71°, is usually smaller than that of tetragonal FE (T-phase FE), in which the dipoles need rotate 90°.[24] Cohen et al. have proposed that polarization rotation along minimum free energy path favors a large piezoelectric response.[25] Therefore, the rotation path in this case may be related to the energy barrier to overcome under the electric field, which can be further supported by the following theory calculations.

More insight on the relationship between rotation angle and energy barrier was gained from density functional theory (DFT) calculations using $PbZrO_3$ as a model. The same method also has been used in other electronic studies.[26−29] To assess the energy barrier of different rotation angles, two paths were selected, one is $[100]_P$ to $[111]_P$ and the other is $[110]_P$ to $[111]_P$ (the details of DFT calculation are provided in Supporting Information). The differences of DFT calculated energies, so-called energy barrier, with respect to different paths are displayed in Figure 5c. Note that the Path-1 has an energy barrier of 45.4 meV/f.u. much higher than that of Path-2 (15.7 meV/f.u.). As expected, this trend is consistent with the change of the rotation angles (as shown in Figure 5b). It is confirmed that a small rotation angle will lead to a small energy barrier, which further will lead to a small critical electric field of AFEs. These results are consistent with the experimental results (Figure 1b).

The above results visually exhibit the process of polarization rotation and reveal the intrinsic correlation between the dipole configuration and the critical electric field of AFEs. Through introducing the rotation angle, the internal determining factor of the critical electric field is found and the FE and AFE theories are well unified by this polarization rotation mechanism. These results clarify the important role of the incommensurate structure in AFEs and offer a picture of the connection between chemical, crystal structure, and functionality.

In summary, we revealed the correlation between the complicated polarization and important macroscopic critical electric field of AFE-to-FE phase transition in AFEs, through quantitative analysis of the modulated structure of Nb-doped $Pb(Zr,Sn,Ti)O_3$ ceramics. The dipole configuration of a series of AFEs was revealed by using HR-NPD refinement, and the polarization jump rotation was observed through synchrotron radiation *in situ* experiments. A rotation angle was introduced to quantitatively estimate the polarization rotation process between the initial (IC AFE) state and the terminal (FE_R) state. The results show that a large rotation angle leads to a large critical electric field. Confirmed by the DFT calculation, a large rotation angle requires a higher energy barrier. It implies that the rotation angle is the determining factor of the macroscopic critical electric field. This work precisely describes the relationship between the incommensurate modulated structure and macroscopic properties of lead-based AFEs, which will lay a foundation for future AFEs research.

■ ASSOCIATED CONTENT

Supporting Information

The Supporting Information is available free of charge at https://pubs.acs.org/doi/10.1021/acs.nanolett.2c04361.

Details for experimental methods for the ceramic sample preparation; neutron powder diffraction data collection; theory calculations; supplementary tables for the crystallography parameters; and supplementary Figures S1−S4 (PDF)

■ AUTHOR INFORMATION

Corresponding Authors

Hui Liu − *Beijing Advanced Innovation Center for Materials Genome Engineering, Department of Physical Chemistry, University of Science and Technology Beijing, Beijing 100083, China; School of Mathematics and Physics, University of Science and Technology Beijing, Beijing 100083, China;* orcid.org/0000-0002-4973-9784; Email: huiliu@ustb.edu.cn

Shi Liu − *Key Laboratory for Quantum Materials of Zhejiang Province, Department of Physics, School of Science, Westlake University, Hangzhou, Zhejiang 310030, China; Institute of Natural Sciences, Westlake Institute for Advanced Study, Hangzhou, Zhejiang 310024, China;* orcid.org/0000-0002-8488-4848; Email: liushi@westlake.edu.cn

Jun Chen − *Beijing Advanced Innovation Center for Materials Genome Engineering, Department of Physical Chemistry, University of Science and Technology Beijing, Beijing 100083, China;* orcid.org/0000-0002-7330-8976; Email: junchen@ustb.edu.cn

Authors

Botao Gao − *Beijing Advanced Innovation Center for Materials Genome Engineering, Department of Physical Chemistry, University of Science and Technology Beijing, Beijing 100083, China; Shanghai Institute of Ceramics, Chinese Academy of Sciences, Shanghai, Shanghai 201899, China*

Wenjie Zhou − *Key Laboratory for Quantum Materials of Zhejiang Province, Department of Physics, School of Science, Westlake University, Hangzhou, Zhejiang 310030, China*

He Qi − *Beijing Advanced Innovation Center for Materials Genome Engineering, Department of Physical Chemistry, University of Science and Technology Beijing, Beijing 100083, China;* orcid.org/0000-0002-3094-3574

Shiqing Deng − *Beijing Advanced Innovation Center for Materials Genome Engineering, Department of Physical Chemistry, University of Science and Technology Beijing, Beijing 100083, China; School of Mathematics and Physics, University of Science and Technology Beijing, Beijing 100083, China;* orcid.org/0000-0001-7016-4084

Complete contact information is available at: https://pubs.acs.org/10.1021/acs.nanolett.2c04361

Author Contributions

B.G., H.L., and J.C. conceived the idea and initiated the research. H.Q. and S.D. supervised the project. W.Z. and S.L. conducted theory calculations and analysis. The ceramic samples were synthesized and measured by B.G., and B.G.

https://doi.org/10.1021/acs.nanolett.2c04361
Nano Lett. 2023, 23, 948−953

performed the data analysis and wrote the manuscript, with help from H.L. and J.C. All authors discussed the results, commented on the manuscript, and have given approval to the final version of the manuscript.

Notes

The authors declare no competing financial interest.

■ ACKNOWLEDGMENTS

This work was supported by the National Natural Science Foundation of China (Grants 22235002, 21825102, and 12004032), the China National Postdoctoral Program for Innovative Talents (Grant BX20200043), and the Fundamental Research Funds for the Central Universities, China (Grant 06500145). The high-resolution neutron diffraction was collected by Dr. Chin-Wei Wang at the National Synchrotron Radiation Research Center. This research used resources of the Advanced Photon Source, a U.S. Department of Energy (DOE) Office of Science User Facility operated for the DOE Office of Science by Argonne National Laboratory under Contract DE-AC02-06CH11357.

■ REFERENCES

(1) Hao, X.; Zhai, J.; Kong, L. B.; Xu, Z. A comprehensive review on the progress of lead zirconate-based antiferroelectric materials. *Prog. Mater. Sci.* **2014**, *63*, 1−57.

(2) Sigman, J.; Norton, D.; Christen, H.; Fleming, P.; Boatner, L. Antiferroelectric behavior in symmetric $KNbO_3/KTaO_3$ superlattices. *Phys. Rev. Lett.* **2002**, *88* (9), 097601.

(3) Wang, G.; Lu, Z.; Li, Y.; Li, L.; Ji, H.; Feteira, A.; Zhou, D.; Wang, D.; Zhang, S.; Reaney, I. M. Electroceramics for high-energy density capacitors: current status and future perspectives. *Chem. Rev.* **2021**, *121* (10), 6124−6172.

(4) Frederick, J.; Tan, X.; Jo, W. Strains and polarization during antiferroelectric-ferroelectric phase switching in $Pb_{0.99}Nb_{0.02}[(Zr_{0.57}Sn_{0.43})_{1-y}Ti_y]_{0.98}O_3$ ceramics. *J. Am. Ceram. Soc.* **2011**, *94* (4), 1149−1155.

(5) Merz, W. J. Domain formation and domain wall motions in ferroelectric $BaTiO_3$ single crystals. *Phys. Rev.* **1954**, *95* (3), 690.

(6) Merz, W. J. Switching time in ferroelectric $BaTiO_3$ and its dependence on crystal thickness. *J. Appl. Phys.* **1956**, *27* (8), 938−943.

(7) Milesi-Brault, C.; Godard, N.; Girod, S.; Fleming, Y.; El Adib, B.; Valle, N.; Glinšek, S.; Defay, E.; Guennou, M. Critical field anisotropy in the antiferroelectric switching of $PbZrO_3$ films. *Appl. Phys. Lett.* **2021**, *118* (4), 042901.

(8) Fu, Z.; Chen, X.; Li, Z.; Hu, T.; Zhang, L.; Lu, P.; Zhang, S.; Wang, G.; Dong, X.; Xu, F. Unveiling the ferrielectric nature of $PbZrO_3$-based antiferroelectric materials. *Nat. Commun.* **2020**, *11* (1), 3809.

(9) Ma, T.; Fan, Z.; Xu, B.; Kim, T.-H.; Lu, P.; Bellaiche, L.; Kramer, M. J.; Tan, X.; Zhou, L. Uncompensated polarization in incommensurate modulations of perovskite antiferroelectrics. *Phys. Rev. Lett.* **2019**, *123* (21), 217602.

(10) Gao, B.; Liu, H.; Zhou, Z.; Deng, S.; Sun, J.; Chen, J. An Intriguing Polarization Configuration of Mixed Ising-and Neel-Type Model in the Prototype $PbZrO_3$-Based Antiferroelectrics. *Inorg. Chem.* **2021**, *60* (5), 3232−3237.

(11) Gao, B.; Liu, H.; Zhou, Z.; Xu, K.; Qi, H.; Deng, S.; Ren, Y.; Sun, J.; Huang, H.; Chen, J. An intriguing canting dipole configuration and its evolution under an electric field in La-doped $Pb(Zr,Sn,Ti)O_3$ perovskites. *Microstructures* **2022**, *2* (2), 2022010.

(12) Berlincourt, D. A. Transducers using forced transitions between ferroelectric and antiferroelectric states. *IEEE Trans. Sonics Ultrason.* **1966**, *13*, 116.

(13) Lyu, C.; Liu, Y.; Lyu, Y.; Qian, H.; Li, M.; Chen, F.; Xi, H. TEM study of incommensurate superstructure in $Pb_{1-0.5x}Nb_x((Zr_{0.52}Sn_{0.48})_{0.955}Ti_{0.045})_{1-x}O_3$ ceramics with 0-1 switching characteristic strain and high energy storage density. *J. Mater. Sci.: Mater. Electron.* **2019**, *30* (13), 12375−12381.

(14) He, H.; Tan, X. Electric-field-induced transformation of incommensurate modulations in antiferroelectric $Pb_{0.99}Nb_{0.02}[(Zr_{1-x}Sn_x)_{1-y}Ti_y]_{0.98}O_3$. *Phys. Rev. B* **2005**, *72* (2), 024102.

(15) Tagantsev, A.; Vaideeswaran, K.; Vakhrushev, S.; Filimonov, A.; Burkovsky, R.; Shaganov, A.; Andronikova, D.; Rudskoy, A.; Baron, A.; Uchiyama, H.; et al. The origin of antiferroelectricity in $PbZrO_3$. *Nat. Commun.* **2013**, *4* (1), 2229.

(16) Sawaguchi, E.; Maniwa, H.; Hoshino, S. Antiferroelectric structure of lead zirconate. *Phys. Rev.* **1951**, *83* (5), 1078.

(17) Yamasaki, K.; Soejima, Y.; Fischer, K. Superstructure determination of $PbZrO_3$. *Acta Crystallogr., Sect. B: Struct. Sci.* **1998**, *54* (5), 524−530.

(18) Jona, F.; Shirane, G.; Mazzi, F.; Pepinsky, R. X-Ray and neutron diffraction study of antiferroelectric lead zirconate, $PbZrO_3$. *Phys. Rev.* **1957**, *105* (3), 849.

(19) Corker, D.; Glazer, A.; Dec, J.; Roleder, K.; Whatmore, R. A re-investigation of the crystal structure of the perovskite $PbZrO_3$ by X-ray and neutron diffraction. *Acta Crystallogr., Sect. B: Struct. Sci.* **1997**, *53* (1), 135−142.

(20) Fan, L.; Chen, J.; Ren, Y.; Pan, Z.; Zhang, L.; Xing, X. Unique Piezoelectric Properties of the Monoclinic Phase in $Pb(Zr, Ti)O_3$ Ceramics: Large Lattice Strain and Negligible Domain Switching. *Phys. Rev. Lett.* **2016**, *116* (2), 027601.

(21) Liu, H.; Chen, J.; Fan, L.; Ren, Y.; Pan, Z.; Lalitha, K.; Rödel, J.; Xing, X. Critical role of monoclinic polarization rotation in high-performance perovskite piezoelectric materials. *Phys. Rev. Lett.* **2017**, *119* (1), 017601.

(22) Liu, H.; Chen, J.; Fan, L.; Ren, Y.; Hu, L.; Guo, F.; Deng, J.; Xing, X. Structural Evidence for Strong Coupling between Polarization Rotation and Lattice Strain in Monoclinic Relaxor Ferroelectrics. *Chem. Mater.* **2017**, *29* (14), 5767−5771.

(23) Fan, L.; Zhang, L.; Liu, H. Direct Observation of Polarization Rotation in the Monoclinic MB Phase under Electrical Loading. *Inorg. Chem.* **2021**, *60* (20), 15190−15195.

(24) Choudhury, S.; Li, Y.; Krill, C., III; Chen, L. Effect of grain orientation and grain size on ferroelectric domain switching and evolution: Phase field simulations. *Acta Mater.* **2007**, *55* (4), 1415−1426.

(25) Fu, H.; Cohen, R. E. Polarization rotation mechanism for ultrahigh electromechanical response in single-crystal piezoelectrics. *Nature* **2000**, *403* (6767), 281−283.

(26) Mundy, J. A.; Grosso, B. F.; Heikes, C. A.; Ferenc Segedin, D.; Wang, Z.; Shao, Y.-T.; Dai, C.; Goodge, B. H.; Meier, Q. N.; Nelson, C. T.; et al. Liberating a hidden antiferroelectric phase with interfacial electrostatic engineering. *Sci. Adv.* **2022**, *8* (5), No. eabg5860.

(27) Bafekry, A.; Stampfl, C.; Ghergherehchi, M.; Shayesteh, S. F. A first-principles study of the effects of atom impurities, defects, strain, electric field and layer thickness on the electronic and magnetic properties of the C_2N nanosheet. *Carbon* **2020**, *157*, 371−384.

(28) Xu, R.; Huang, J.; Barnard, E. S.; Hong, S. S.; Singh, P.; Wong, E. K.; Jansen, T.; Harbola, V.; Xiao, J.; Wang, B. Y.; et al. Strain-induced room-temperature ferroelectricity in $SrTiO_3$ membranes. *Nat. Commun.* **2020**, *11* (1), 3141.

(29) Bafekry, A.; Shayesteh, S. F.; Peeters, F. M. Introducing novel electronic and magnetic properties in C_3N nanosheets by defect engineering and atom substitution. *Phys. Chem. Chem. Phys.* **2019**, *21* (37), 21070−21083.

https://doi.org/10.1021/acs.nanolett.2c04361
Nano Lett. 2023, 23, 948−953